JOURNAL OF MATERIALS SCIENCE **40** (2005) 933–942

Bulk and surface structures of iron doped zirconium oxide systems: Influence of preparation method

F. WYRWALSKI, J. F. LAMONIER*, S. SIFFERT, E. A. ZHILINSKAYA
Laboratoire de Catalyse et Environnement, E.A. 2598, MREI, Université du Littoral - Côte d'Opale, 145, Avenue Maurice Schumann, 59140 Dunkerque, France
E-mail: lamonier@univ-littoral.fr

L. GENGEMBRE
Laboratoire de Catalyse de Lille, UMR 08010, Université des Sciences et Technologies de Lille, 59650 Villeneuve d'Ascq, France

A. ABOUKAÏS
Laboratoire de Catalyse et Environnement, E.A. 2598, MREI, Université du Littoral - Côte d'Opale, 145, Avenue Maurice Schumann, 59140 Dunkerque, France

Three different Fe-Zr oxide systems were prepared using firstly classical impregnation of iron nitrates on calcined ZrO_2 (Fe_x/ZrO_2, x represents Fe/Zr ratio = 0.01 and 0.11), secondly impregnation of iron nitrates on dried zirconium hydroxide $ZrO(OH)_2$ ($Fe_x/ZrO(OH)_2$) and finally hydrolysis of aqueous suspension of iron and zirconium salts to coprecipitate iron and zirconium hydroxides (Fe_x-Zr). Thermal decomposition study of dried samples evidenced a delay in the temperature crystallization of zirconia for Fe_x-Zr and $Fe_x/ZrO(OH)_2$, the more the iron content in the sample, the more important the delay. For these samples, the formation and the stabilization of different phases were evidenced by several characterization techniques : X-Ray Diffraction (XRD), Raman spectroscopy and Electron Paramagnetic Resonance (EPR).

The interaction of iron species with zirconia was different in accordance with different preparations. A bulk dispersion of the coprecipitated sample was observed and as a consequence Zr^{3+} defects in the solid were not produced. In the case of Fe_x/ZrO_2 sample, production of surface Zr^{3+} ions was established at low temperature of calcination (up to 600°C) and explained by the reaction of NO_3^- with Zr^{4+} on the zirconia surface. However such interaction did not occur for $Fe_x/ZrO(OH)_2$ since a low dispersion of iron species was observed by X-ray Photoelectron Spectroscopy (XPS), deposited phase (Fe_2O_3) forming preferentially blocks. Temperature Programmed Reduction (TPR) showed that the reduction of small particles of Fe_2O_3 and bulk Fe_2O_3 present in the impregnated samples was easier than that of iron species well dispersed in the bulk of the coprecipitated solid.

1. Introduction

Zirconium dioxide or zirconia (ZrO_2) is an interesting material used in catalysis. Due to its nature of *n*-type semiconductor, ZrO_2 shows photocatalytic activity in reactions of liquide-phase oxidation of some organic substrates [1, 2]. Moreover lability and easiness to exchange oxygen atoms of the tetragonal or cubic ZrO_2 phase make them suitable for numerous catalytic reactions [3]. However the tetragonal or cubic phase of pure zirconia is only stabilized at high temperatures (up to 1900°C). The stabilization of the high temperature phases (cubic or tetragonal at room temperature) is possible by introducing in the ZrO_2 structure suitable aliovalent cations such as Ca^{2+}, Mg^{2+}, Gd^{3+} and Y^{3+} (oversized dopants: ionic radii bigger than Zr^{4+} radius) [4]. In these conditions, oxide ion conductor with high ionic conductivity is obtained. In fact the substitution of Zr^{4+} by cations having a lower charge results in the creation of oxygen vacancies in order to maintain the charge balance. The concentration of the stoechiometric oxygen vacancies equals to half of the concentration of the aliovalent cation which substitues the Zr ions [5]. The incorporation of Fe^{3+} cations induces also a stabilization of high temperature phase of zirconia, but the

*Author to whom all correspondence should be addressed.

use of undersized dopants (for example Fe^{3+} or Ga^{2+}) leads to a less efficient stabilization. As a function of air pressure used for the calcination, Stefanic *et al.* [6] showed that the incorporation of Fe^{3+} into ZrO_2 have both a stabilizing and destabilizing influence on the high temperature phase of zirconia.

For Fischer-Tropsch synthesis iron is chosen as the active metal for its ability to dissociatively adsorb CO faster than H_2 which enhances the olefinic selectivity [7]. Moreover ZrO_2-supported Fe oxides have been shown to be highly active at low temperature in CO+NO reaction and in oxidation of CO [8]. Furthermore, catalysts promoted with iron and manganese were reported to be 3 orders of magnitude more active that conventional sulfated zirconia for n-butane isomerization [9]. But the nature of the promoting of these transition metals remains controversal. Using zirconia as support, the stabilization of its tetragonal phase is often mentioned to explain the superiority of the catalyst in terms of activity or selectivity. The interaction of active species with the support is also stated to make clear the catalytic results [10]. But this stabilization and this interaction strongly depend on the preparation method of the sample. For sulfated zirconia catalysts promoted with iron, iron is deposited either on sulfate-ion-treated $Zr(OH)_4$ [11] or, previous the sulfation, on pure zirconium hydroxide $Zr(OH)_4$ [12] using incipient wetness impregnation with $Fe(NO_3)_3$ aqueous solution. Besides the direct impregnation of Cu on zirconium hydroxyde $ZrO(OH)_2$ leads to an effective catalyst in the propene oxidation [13] having higher catalytic activity than that measured with classical Cu/ZrO_2. However the direct deposition of palladium on $ZrO(OH)_2$ leads to a less active catalyst for the Fischer-Tropsch reaction due to bigger PdO particles formation compared with those obtained after deposition of palladium on ZrO_2 previously calcined [14].

The purpose of this work is to compare the influence of iron species onto zirconium oxides structure developing three different experimental procedures for the Fe-Zr oxide synthesis. The classical impregnation of iron salt on calcined ZrO_2 has been first employed. The hydrolysis of aqueous suspension of iron and zirconium salts was secondly employed to coprecipitate iron and zirconium hydroxides. Dried $ZrO(OH)_2$ support has been thirdly used to add iron species. *In situ* thermal analyses like Differential Thermal Analysis (DTA) and Temperature Programmed Reduction (TPR) allow to respectively evidence the crystallization of zirconia (exothermic phenomenon) and the type of iron species (reduction at different temperatures of different types). X-Ray Diffraction (XRD) and Raman spectroscopy give much information about the structure of molecules and crystals and these investigations provide the information mainly on the bulk of zirconia. The transformation from the metastable tetragonal phase to the monoclinic phase of crystalline ZrO_2 starting from the surface region of the particle and extending into the bulk [15], X-ray Photoelectron Spectroscopy (XPS) has been also performed in order to study the surface of the different Fe-Zr systems. The high sensitivity of Electron Paramagnetic Resonance (EPR) has been used to evidence the phase change, the interaction between iron species and zirconia and Fe^{3+} state as a function of the preparation method.

2. Experimental procedure

2.1. Samples preparation

Zirconium hydroxide was prepared by adding drop by drop an aqueous ammonium hydroxide (0.7 M) to a known solution of zirconium oxychloride $ZrOCl_2$, $8H_2O$ (0.15 M) up to pH = 9.8. Thereafter, the precipitated hydroxide ($ZrO(OH)_2$) was filtered, washed and dried at 100°C before a calcination treatment in a flow of dried air (2 $L{\cdot}h^{-1}$) during 4 h at a given temperature. The same procedure was used to prepare zirconium and iron mixed hydroxides: a known solution of $ZrOCl_2$, $8H_2O$ (0.15 M) and $Fe(NO_3)_3$, $9H_2O$ was added to an aqueous ammonium hydroxide (0.7 M). Different Fe_x-Zr solids were then synthesized where x is the value of Fe/Zr atomic ratio (0.01 or 0.11). The impregnated method was also employed to deposit iron on ZrO_2 ($ZrO(OH)_2$ calcined at 600°C) or directly on $ZrO(OH)_2$ (not calcined) named respectively Fe_x/ZrO_2 and $Fe_x/ZrO(OH)_2$ where x is the value of Fe/Zr atomic ratio (0.01 and 0.11). After introduction of iron species, the samples were calcined at different temperatures.

A chemical analysis of zirconium oxychloride precursor revealed the presence of iron impurities (∼1 ppm). Chemical analyses of the different samples give the Fe/Zr expected atomic ratio.

2.2. Samples characterization

The specific areas of solids were determined by the BET method using a Quantasorb Junior apparatus, and the gas adsorbed at −196°C was pure nitrogen.

DTA (Netzsch STA 409 equipped with a microbalance) was conducted in flow air (75 $mL \cdot min^{-1}$) at a heating rate of 5°C min^{-1} from room temperature to 700°C (mass of sample = 50 mg).

The structures of solids were analyzed at room temperature by XRD technique in a Bruker D8 diffractometer equipped with a copper anode ($\lambda = 1.5418$ Å). The scattering intensities were measured over an angular range of $10^\circ < 2\Theta < 80^\circ$ for all the samples with a step-size of $\Delta(2\Theta) = 0.03^\circ$ and a count time of 4s per step. The diffraction spectra have been indexed by comparison with the JCPDS files.

The Raman spectra were recorded using a Dilor XY monochromator with substractive dispersion. The samples were excited using 632.8 nm radiation of a He-Ne laser.

X-Ray photoelectron spectra of the catalyst samples were recorded using a VG instrument (anode operated at 12 kV and 25 mA with fixed analyser transmission mode) equipped with an aluminum anode ($h\nu = 1486.6$ eV). The samples were deposited on an indium support and the working pressure in the analysis chamber was maintained at around 10^{-7} mbar. Charging effects were corrected using C1s peak at binding energy of 285 eV. Surface atomic ratios were obtained on the basis of the peak area intensities after correction for instrumental

parameters, photoionization cross sections and electron mean free paths.

TPR experiments were carried out in a conventional instrument (AMI 200 from ZETON ALTAMIRA). Before the reduction, all catalysts were in situ actived at 150°C (heating rate 5°C/min) with a constant flow rate of pure argon (30 mL/min). Thereafter, samples (100 or 200 mg) were heated from 30°C to 1000°C (heating rate 5°C/min) under reducing gas (3%vol H_2/Ar) with a constant flow rate of 30 mL/min.

EPR measurements were performed at 20 and −196°C on an EMX Bruker spectrometer. A cavity operating with a frequency of 9.3 GHz (X-band) is used. The magnetic field is modulated at 100 kHz. Precise g values were determined from simultaneous precise frequency and magnetic field values. All EPR spectra were treated using Bruker WINEPR program. Relative amounts of paramagnetic species, Ns, were estimated using the normalized double integration. The proportion of superposed EPR signals was estimated calculating the ratio value of amplitude of non superposed parts of the corresponding signals.

3. Results and discussion

The thermal decomposition of the dried zirconium hydroxide $ZrO(OH)_2$ has been presented in a previous paper in the same experimental conditions [16]. The complete dehydration of solid was achieved at 450°C. An exothermic DTA signal was observed at 419°C (without loss of weight). This signal was attributed to the crystallization of amorphous ZrO_2 into tetragonal phase ZrO_2.

For $Fe_x/ZrO(OH)_2$ and Fe_x-Zr dried samples, the exothermic DTA peak is always present but the maximum is shifted at higher temperature (Fig. 1). Comparing the both preparation method, the delay in the crystallization of zirconia is more pronounced when iron hydroxide is coprecipitated with zirconium hydroxide. Indeed $Fe_{0.11}/ZrO(OH)_2$ and $Fe_{0.11}$-Zr solids exhibit respectively a DTA signal at maximum temperature of 451°C and 511°C. Moreover the more the iron content in the sample, the more important is the delay of crystallization temperature.

These results can be partially connected to the BET data (Fig. 2). $Fe_x/ZrO(OH)_2$ and Fe_x-Zr samples present higher specific area values in comparison with those obtained for pure ZrO_2 and iron supported ZrO_2. The increase of iron content in the $Fe_x/ZrO(OH)_2$ and Fe_x-Zr samples leads to higher specific area according to a lower zirconia crystallization. However the specific area values do not follow in a straight line with the temperature of zirconia crystallization. Therefore the formation of iron oxide phase, which contributes to the specific area value, can be suggested. In order to evidence the formation of such phase, XRD and Raman spectroscopy have been performed.

Fig. 3 shows the evolution of the XRD patterns recorded at room temperature of the coprecipited and impregnated samples ($x = 0.11$) calcined at 600°C. The lines at $2\theta = 30.4°$ and 35.3° indicate the presence of ZrO_2 into the tetragonal (JCPDS no. 80 2156) or cubic phases. The tetragonal structure can be distinguished from the cubic structure by the presence of a characteristic splitting of the diffraction peaks. But at high angles where the angular separation $\Delta(2\Theta)$ is greater, the tetragonal doublet (004)-(400) is not clearly observed due to the low intensities of these lines. The Laser Raman spectroscopy allows discriminating the tetragonal structure from the cubic one [17]. Single Raman band located at around 460 cm^{-1} and characteristic of the cubic structure (fluorite) has not been observed in our samples. These results indicate that zirconia rather crystallizes in the tetragonal form (marked T). The lines at 28.5°, 31.5° and 34.4° are attributed to zirconia in the monoclinic form (marked M ; JCPDS no. 78 0047). The percentage of the tetragonal phase decreases according to the following sequence : $Fe_{0.11}$-Zr > $Fe_{0.11}/ZrO(OH)_2$ > $Fe_{0.11}/ZrO_2$. The XRD pattern of $Fe_{0.11}/ZrO_2$ is identical of pure ZrO_2 calcined at 600°C suggesting that addition of iron at the surface of zirconia already calcined do not modified its structure. The more important stabilization in the tetragonal phase observed in $Fe_{0.11}$-Zr and $Fe_{0.11}/ZrO(OH)_2$ samples can be explained by the higher temperature crystallization of zirconia which delay the transformation of the tetragonal phase into the monoclinic one. For $Fe_{0.11}/ZrO(OH)_2$ sample another crystalline phase is observed (2Θ = 33.3°) and is assigned to Fe_2O_3 (marked F; JCPDS no. 80 307).

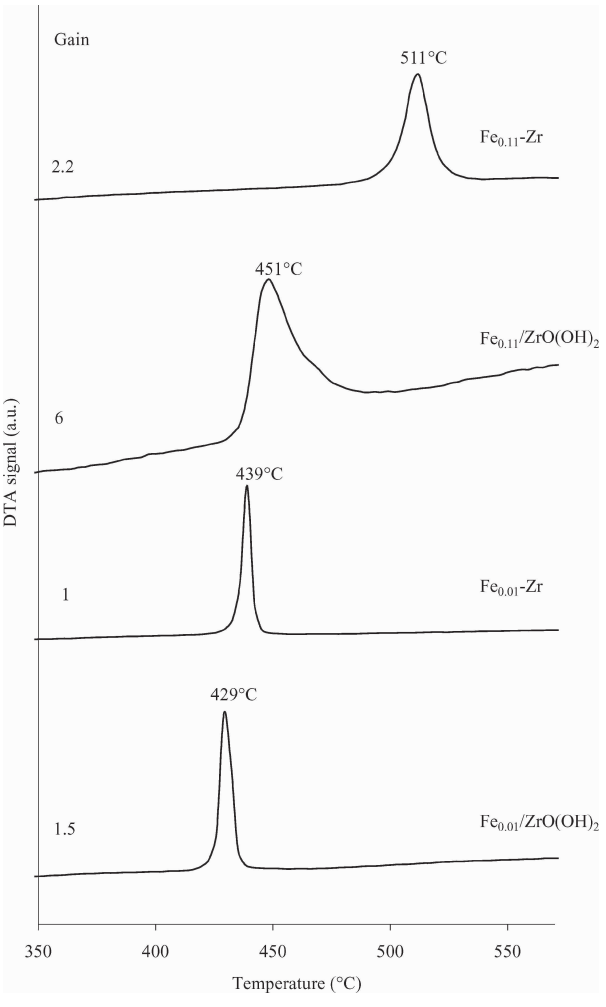

Figure 1 DTA signals obtained during the calcination of pure $ZrO(OH)_2$, $Fe_x/ZrO(OH)_2$ and Fe_x-Zr.

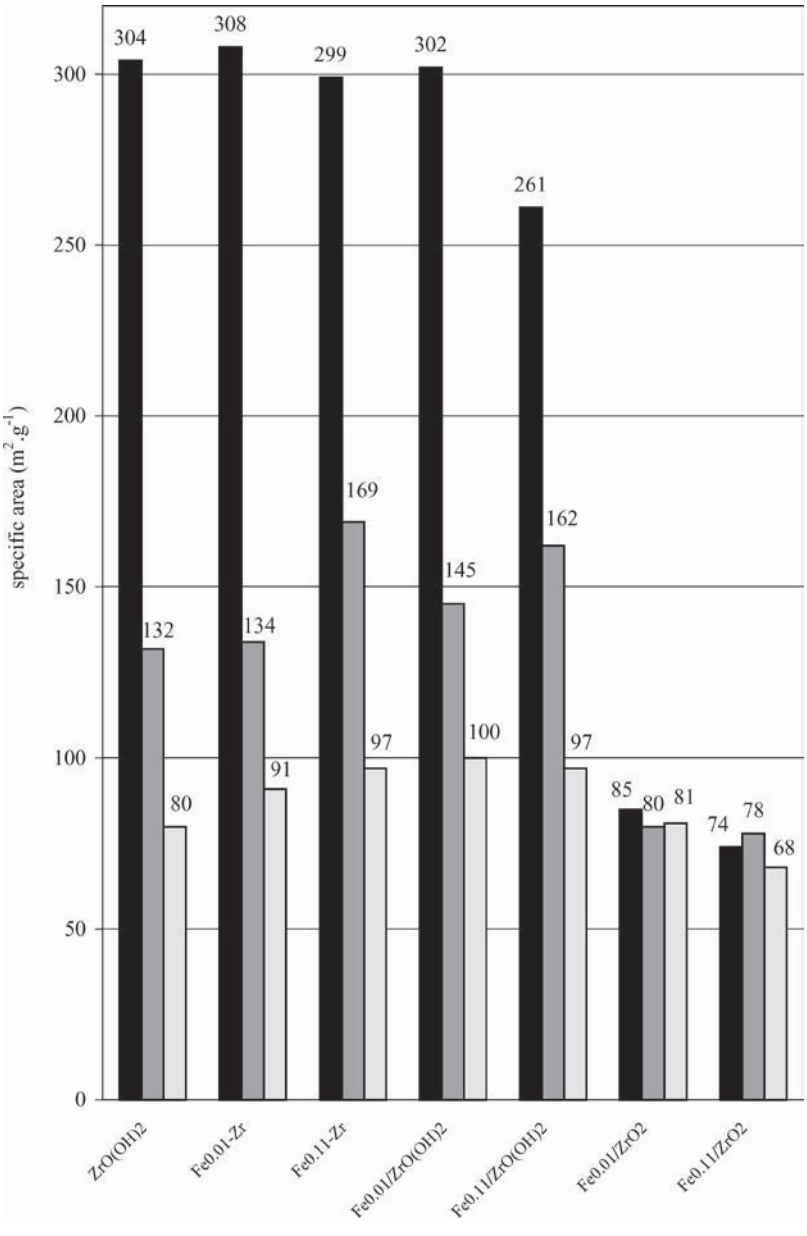

Figure 2 Surface specific areas for pure $ZrO(OH)_2$, Fe_x/ZrO_2, $Fe_x/ZrO(OH)_2$ and Fe_x-Zr dried (■), calcined at 450°C (▒) and 600°C (▒).

The Raman study of the same samples confirms XRD results: stabilization of the tetragonal phase of zirconia in $Fe_{0.11}$-Zr and $Fe_{0.11}/ZrO(OH)_2$ samples and Fe_2O_3 concentration higher for $Fe_{0.11}/ZrO(OH)_2$ than for $Fe_{0.11}/ZrO_2$.

For $x = 0.01$, XRD study reveals also a stabilization of ZrO_2 into the tetragonal phase. But according to lower crystallization temperature obtained for $x = 0.01$, the percentage of the tetragonal phase is lower than that measured for $x = 0.11$. No crystalline phase of Fe_2O_3 is observed in the case of this low iron content.

The Raman spectra of ZrO_2, $Fe_{0.01}/ZrO_2$, $Fe_{0.01}/ZrO(OH)_2$ and $Fe_{0.01}$-Zr calcined at 600°C are shown in Fig. 4. As observed by XRD, the classical impregnation of iron on ZrO_2 does not modify the structure of the support zirconia (monoclinic (M) and tetragonal (T) phases). The stabilization of the tetragonal phase is observed for $Fe_{0.01}$-Zr and $Fe_{0.01}/ZrO(OH)_2$ since the intensity of bands at 277 cm^{-1} and 325 cm^{-1} characteristic of the tetragonal structure increases [18]. The Raman spectrum of Fe_2O_3 compound, obtained after calcination at 600°C of FeO(OH), is also presented on the figure as a reference and because some of its spectral features (especially 296 cm^{-1} and 413 cm^{-1}) are the same that those additional bands observed when iron species are supported. Fe_2O_3 concentration is higher when nitrate iron is initially deposited on $ZrO(OH)_2$ rather than on ZrO_2. For $Fe_{0.01}$-Zr no trace of Fe_2O_3 is detected by Raman spectroscopy.

On the contrary to XRD analyses, Raman spectroscopy allows to evidence Fe_2O_3 formation for supported samples with low iron content ($x = 0.01$).

The surface composition of our samples was evaluated using X-ray photoelectron spectroscopy. The analyses were obtained by elaboration of the Zr 3d, O 1s and Fe 2p spectral regions. The binding energy (BE) values (reference BE of C 1s at 285 eV), are listed in Table I. Zr $3d_{5/2}$ BE at around 182 eV is typically associated with zirconium in ZrO_2 sample [19, 20]. Oxygen 1s peaks show, in any case, the presence of reticular O^{2-} (photoelectron emission at around 529.8 eV

TABLE I XPS Binding energies (eV) of Zr $3d_{5/2}$, O 1s and Fe $2p_{3/2}$ and atomic surface composition of different iron based samples

	XPS Binding energies (eV)			Fe/Zr		O/Zr	
Sample	Zr $3d_{5/2}$	O 1s	Fe $2p_{3/2}$	Bulk	Surface	Bulk	Surface
$Fe_{0.11}/ZrO(OH)_2$ (600)	182.2	529.4	710.2	0.11	2.97	2.86	5.07
$Fe_{0.11}/ZrO_2$ (600)	181.9	529.8	710.3	0.11	0.86	2.49	2.70
$Fe_{0.11}$-Zr (600)	182.1	529.9	710.8	0.11	0.15	2.61	2.19
$Fe_{0.11}$-Zr (450)	181.9	529.8	710.7	0.11	0.12	2.61	2.08
$Fe_{0.11}$-Zr (1000)	182.0	529.9	711.1	0.11	0.23	2.61	2.12

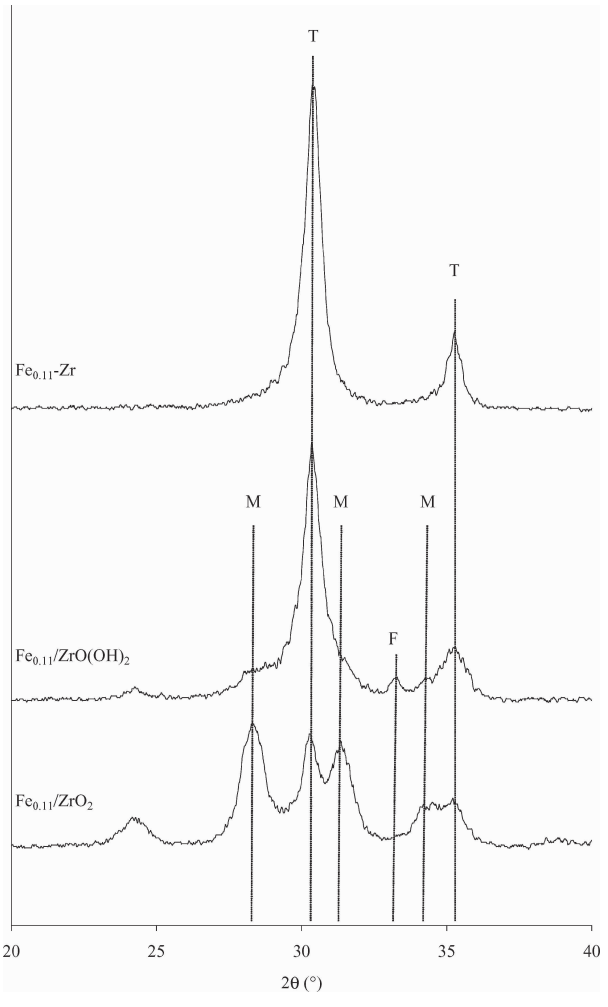

Figure 3 XRD patterns of $Fe_{0.11}/ZrO_2$, $Fe_{0.11}/ZrO(OH)_2$ and $Fe_{0.11}$-Zr calcined at 600°C; M: ZrO_2 monoclinic phase; T: ZrO_2 tetragonal phase; F: Fe_2O_3 phase.

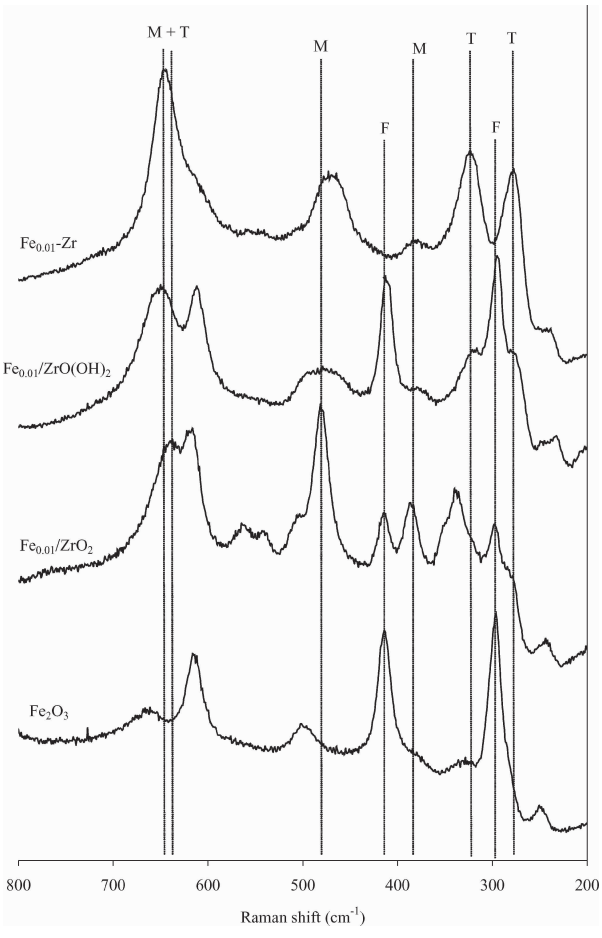

Figure 4 Raman spectra of Fe_2O_3, $Fe_{0.01}/ZrO_2$, $Fe_{0.01}/ZrO(OH)_2$ and $Fe_{0.01}$-Zr calcined at 600°C; M: ZrO_2 monoclinic vibration; T: ZrO_2 tetragonal vibration; F: Fe_2O_3 vibration.

characteristic of O 1s in ZrO_2 sample [21]) and OH groups and/or chemisorbed water (shoulder at around 532 eV). Some differences are observed studying the iron species since the Fe $2p_{3/2}$ BE varies from 710.2 to 711.1 eV. Brundle *et al.* [22] have shown that in bulk iron oxides (Fe_2O_3, Fe_3O_4, FeO(OH) or Fe_xO) Fe(III) has a $2p_{3/2}$ BE of around 711 eV whereas, the $2p_{3/2}$ BE of Fe(II) is rather centered at around 709.7 eV. The discrimination between Fe(III) and Fe(II) species makes easier taking into consideration the shake-up satellite energy. Indeed this satellite structure is centered at 719.8 eV or 715 eV for respectively Fe(III) or Fe(II) [23]. For all the coprecipitated or supported iron samples, satellite peak at around 719 eV was observed indicating the presence of Fe(III) at the surface. So the binding energy variation observed for Fe $2p_{3/2}$ core levels (Table I) is probably due to different chemical environments of Fe(III) ions.

The lower value of O 1s at 529.4 eV for $Fe_{0.11}/ZrO(OH)_2$ is well explained if oxygen signal is mainly due to the presence at the surface of Fe_2O_3 phase. Indeed, studying different metal oxides (in the same experimental conditions), Wagner *et al.* [24] observed a lower binding energy of 0.8 eV for O 1s from Fe_2O_3 in comparison with O 1s from ZrO_2.

In Table I, the atomic surface and bulk compositions are presented. For the coprecipitated sample, the quantitative analysis reveals an homogeneous distribution of iron in the solid since the surface Fe/Zr ratio is closed to the bulk one (Table I). But when the calcination temperature increases, the XPS Fe/Zr ratio enhances gradually, indicating iron species migration at the surface in relation to zirconium. The O/Zr ratio of ~2 is in

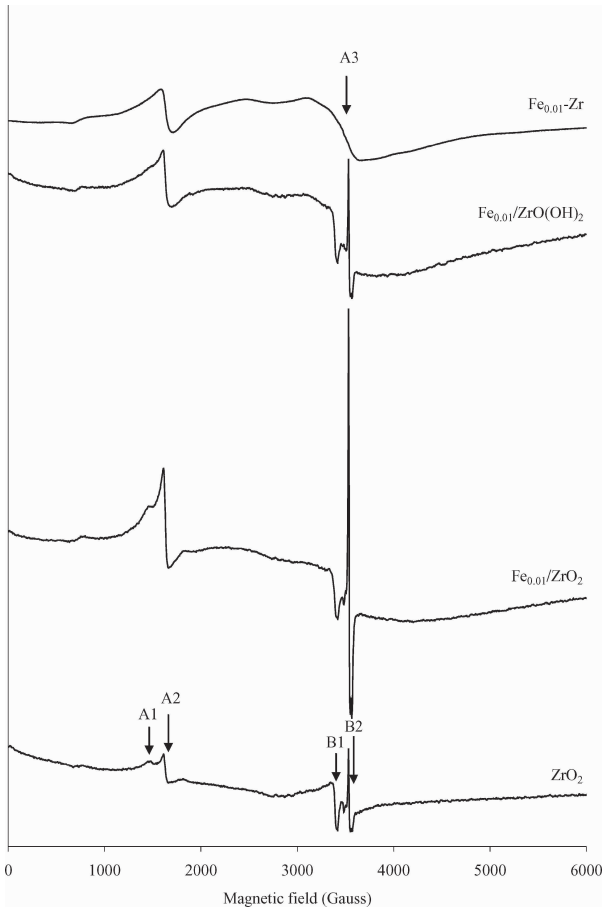

Figure 5 EPR spectra (recorded at room temperature) of ZrO_2, $Fe_{0.11}/ZrO_2$, $Fe_{0.11}/ZrO(OH)_2$ and $Fe_{0.11}$-Zr calcined at 600°C.

agreement with the ZrO_2 formation. Consistent with the impregnation method, iron enrichment is observed for the both supported samples. For $Fe_{0.11}/ZrO(OH)_2$, the XPS O/Fe ratio equal to 1.71 is in agreement with the major presence of Fe_2O_3 at the surface. However the iron enrichment is striking because the Fe/Zr ratio increases 26 times (7.8 times for $Fe_{0.11}/ZrO_2$). This strong enrichment could be explained by a change in the mode of the Fe_2O_3 dispersion on the ZrO_2 surface. The higher enrichment for $Fe_{0.11}/ZrO(OH)_2$ is well explained if the deposited phase forms preferentially blocks of different height (at low content some fraction of the support could remained uncovered) rather than covers of the support to lead uniform deposition ($Fe_{0.11}/ZrO_2$).

So the more visible bands of Fe_2O_3 (Raman) and diffraction lines of Fe_2O_3 (XRD) observed for $Fe_{0.11}/ZrO(OH)_2$ than for $Fe_{0.11}/ZrO_2$ is probably due to a lower dispersion of iron species on the zirconia surface using this method of preparation.

Fig. 5 depicts the EPR spectra of ZrO_2, Fe_x/ZrO_2, $Fe_x/ZrO(OH)_2$ and Fe_x-Zr for $x = 0.01$ and calcined at 600°C. Around 1500 G, two signals (A1 and A2) with g values ($g_1 = 4.80$ and $g_2 = 4.27$) are clearly observed and assigned to isolated Fe^{3+} ions [25] with two different symmetries. Indeed it has already been shown [16] that the Fe^{3+} ions present in ZrO_2 structure as impurities can be used as probes to follow the change in the zirconia change. Similar signals have been obtained and attributed to the presence of iron in a monoclinic ($g_1 = 4.80$) and tetragonal environment ($g_2 = 4.27$). So, iron species added are present in two different types of sites in different proportions (excepted for $Fe_{0.01}$-Zr solid). Table II shows the values of the ratio of A1 and A2 signals amplitudes ($I_{(A1)}/I_{(A2)}$) as a function of the preparation method and the calcination temperature (600 and 1000°C). These results confirm the higher stabilization of the tetragonal phase for $Fe_x/ZrO(OH)_2$ and Fe_x-Zr samples in comparison with pure ZrO_2 and Fe_x/ZrO_2 observed previously by XRD and Raman spectroscopy. EPR results indicate also that higher temperature of calcination (1000°C) leads to the partial transformation of the tetragonal ZrO_2 phase into the monoclinic one. This transformation has already been observed using XRD or Raman spectroscopy for pure zirconia [16].

For $Fe_{0.01}$-Zr sample, a second signal is clearly observed around 3500 G ($g_3 = 2.1$). This signal, denoted A3, can be attributed to the presence of Fe^{3+} in interaction [26].

For ZrO_2, $Fe_{0.01}/ZrO_2$ and $Fe_{0.01}/ZrO(OH)_2$ samples, around 3500 G, the spectrum is also the superposition of two signals, denoted B1 and B2. The B1 signal ($g = 2.06$) is attributed to the perpendicular component of EPR spectrum of Cu^{2+} ions present as impurities in the solid. The B2 signal (see also Fig. 6) of axial symmetry ($g_\perp = 1.979$ and $g_{//} \sim 1.96$) is assigned to Zr^{3+} ions which are presented as defects in solids that should mainly contain Zr^{4+} ions (ZrO_2) [27]. Zr^{3+} cations were not detected by XPS analysis probably because of their low concentration. They can be identified only by EPR spectroscopy, which is a more sensitive technique and which detects only paramagnetic species, i.e., Zr^{3+} and not Zr^{4+}. The presence of Zr^{3+} ions has been associated to the occurrence of anionic vacancies. Indeed O^{2-} vacancies ($V(O^{2-})$) and Zr^{3+} formation are usually described by the following reactions [28]:

$$O^{2-} \Leftrightarrow \frac{1}{2}\, O_2 + V(O^{2-}) + 2e^- \qquad (1)$$

$$Zr^{4+} + e^- \Leftrightarrow Zr^{3+} \qquad (2)$$

Fig. 6 shows EPR spectra (only B2 signal assigned previously to Zr^{3+} ions) of $Fe_{0.01}/ZrO(OH)_2$ samples calcined at different temperatures and recorded at −196°C. For the sample calcined at 450°C, large signal with approximate $g_{//}$ value of 1.960 is measured. The difference observed in $g_{//}$ value for this temperature of calcination, in comparison with that obtained at higher

TABLE II $I_{(A1)}/I_{(A2)}$ ratio as a function of the preparation method and calcination temperature

Sample	$ZrO(OH)_2$		$Fe_{0.01}/ZrO_2$		$Fe_{0.01}/ZrO(OH)_2$		$Fe_{0.01}$-Zr	
Calcination temperature (°C)	600	1000	600	1000	600	1000	600	1000
$I_{(A1)}/I_{(A2)}$ ratio	0.25	0.72	0.22	0.67	0.12	0.54	0	0.43

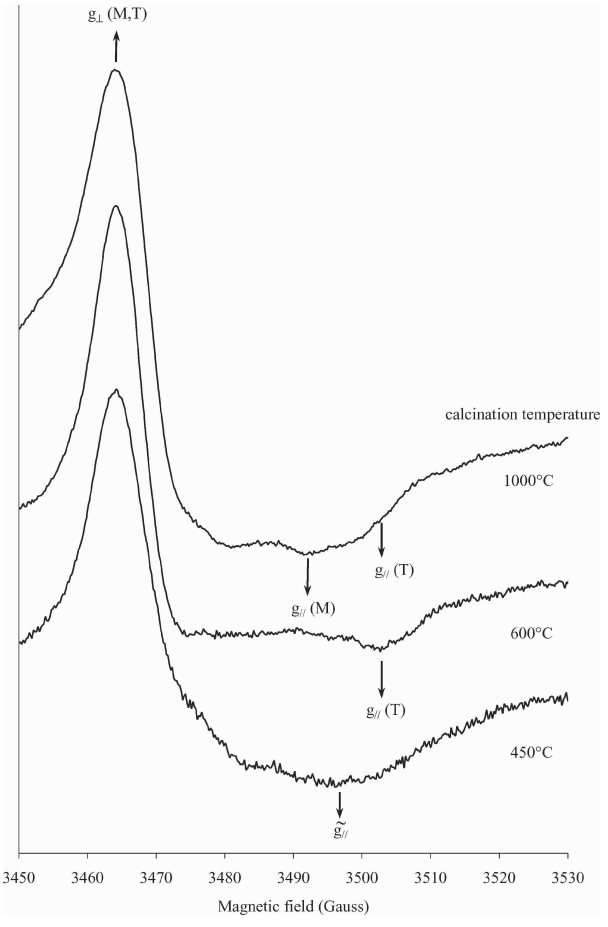

Figure 6 EPR spectra (recorded at −196°C) of $Fe_{0.11}/ZrO(OH)_2$ as a function of calcination temperature.

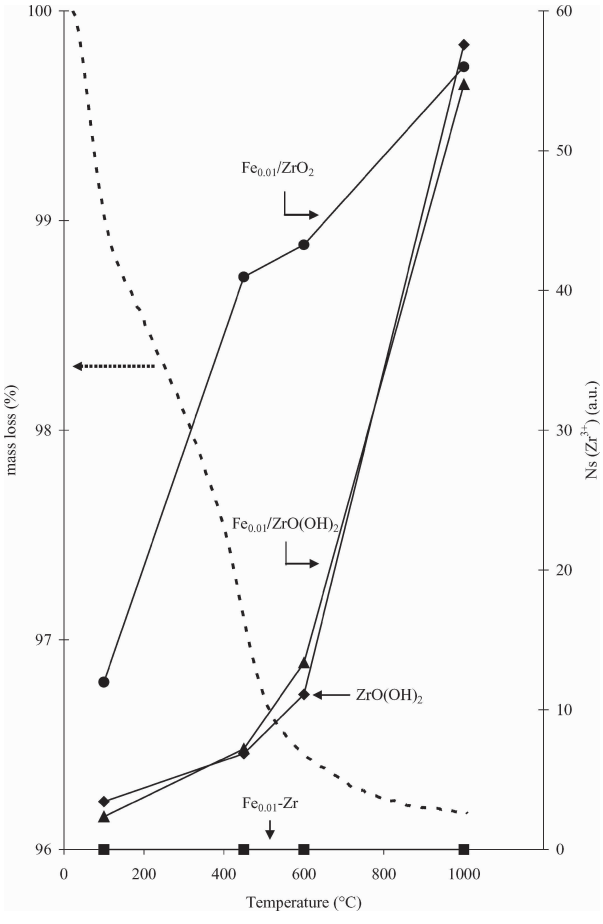

Figure 7 Evolution of amount of Zr^{3+} species (Ns (Zr^{3+})) as a function of calcination temperature (single lines) and mass loss (%) obtained during the calcination of dried $Fe_{0.01}/ZrO_2$ (dotted underline).

temperatures (see below), can be connected to the zirconia structure. Indeed with reference to pure $ZrO(OH)_2$, a delay of crystallisation temperature of about 30°C for $Fe_{0.01}/ZrO(OH)_2$ sample has been observed and at 450°C zirconia is still probably in amorphous phase or low crystallized.

Contrary to $g_\perp$ ($g_\perp$(M,T) = 1.979 for all temperatures of calcination), two different $g_{//}$ values are observed for calcination temperature of 600 and 1000°C. These signals were earlier studied in pure ZrO_2 [29] and assigned to Zr^{3+} ions in monoclinic ($g_\perp$(M) = 1.979; $g_{//}$ (M) = 1.964) and tetragonal ($g_\perp$(T) = 1.979; $g_{//}$ (T) = 1.957) environment. For $Fe_{0.01}/ZrO(OH)_2$ calcined at 600°C, Zr^{3+} ions are essentially located in tetragonal environment. But increasing the temperature, the transformation of the ZrO_2 tetragonal phase into the monoclinic one takes place since the parallel component of Zr^{3+} in monoclinic environment ($g_{//}$ (M)) predominates at 1000°C. Moreover, the comparison of the Zr^{3+} EPR signals obtained for $Fe_{0.01}/ZrO(OH)_2$ and for $Fe_{0.01}/ZrO_2$ samples at the same temperature confirms the higher stabilization of the tetragonal zirconia phase (in relation to the monoclinic one) when iron species are deposited on $ZrO(OH)_2$. Indeed at 600 and 1000°C, the ratio of parallel component amplitudes of Zr^{3+} in a monoclinic environment and Zr^{3+} in a tetragonal environment is lower for $Fe_{0.01}/ZrO(OH)_2$ than for $Fe_{0.01}/ZrO_2$. Finally let us note that for $Fe_{0.01}/ZrO_2$ sample, the Zr^{3+} EPR spectrum is similar for 450 and 600°C according to the previous calcination of the support ZrO_2 at 600°C.

Fig. 7 depicts the evolution of relative amounts of Zr^{3+} (Ns (Zr^{3+})) versus calcination temperature for pure $ZrO(OH)_2$ and for Fe/Zr = 0.01 samples. For pure $ZrO(OH)_2$, slight increase of Zr^{3+} concentration is first observed. In fact the departure of OH^-, during the dehydration of zirconium hydroxide, can reduce some Zr^{4+} ions into Zr^{3+} before the formation of ZrO_2 and H_2O. During the dehydration, a first mechanism of Zr^{3+} creation can be proposed according the following reaction:

$$2\,Zr^{4+} + 2\,OH^- \rightarrow 2\,Zr^{3+} + H_2O + \frac{1}{2}\,O_2(g) \qquad (3)$$

At higher temperatures (600 and 1000°C), the Zr^{3+} formation becomes more significant but we must exclude the participation of OH^-. Indeed in this temperature range the thermal decomposition of $ZrO(OH)_2$ into ZrO_2 is complete and then Zr^{3+} formation is associated to the transformation of the zirconia tetragonal phase into the monoclinic one.

For $Fe_{0.01}/ZrO_2$, dried at 100°C, the quantity of Zr^{3+} defects is similar to that observed for $ZrO(OH)_2$ calcined at 600°C. This result indicates that impregnation of $Fe(NO_3)_3$ solution followed by a drying at 100°C does not modify the support ZrO_2 already calcined at 600°C. However a further calcination up to 600°C leads to a significant increase of Zr^{3+} quantity, higher than these achieved for pure $ZrO(OH)_2$

and $Fe_{0.01}/ZrO(OH)_2$ solids. This result suggests reaction between surface deposited species and the support ZrO_2 which only takes place during the decomposition of iron salt and the iron oxide formation. Zr^{3+} species are probably partly superficial. Indeed, as it has been observed that the temperature range 100–600°C corresponds to the decomposition of $Fe(NO_3)_3/ZrO_2$ (observed by thermogravimetric analysis), one may suggest the following reaction at the surface of zirconia:

$$Zr^{4+}_{(surf)} + NO_3^- \rightarrow Zr^{3+}_{(surf)} + NO(g) + O_2(g) \qquad (4)$$

This hypothesis is emphasized since high mass loss (100–450°C) corresponds to high Zr^{3+} formation whereas low mass loss (450–600°C) matches well with low Zr^{3+} creation. Besides, in order to explain the formation of Zr^{3+} ions in the sulfated zirconia, Chen *et al.* [30] have suggested the reduction of Zr^{4+} into Zr^{3+} species by SO_4^{2-} ions.

When iron hydroxide is coprecipitated with zirconium hydroxide Zr^{3+} defects are not created whatever the temperature of calcination. The reduction of Zr^{4+} into Zr^{3+} by the released electrons (reaction (2)) does not occur in the presence of Fe^{3+} ions well dispersed in the bulk. In fact Fe^{3+} ions must be preferentially reduced in comparison with Zr^{4+} according to the following reaction:

$$Fe^{3+} + e^- \Leftrightarrow Fe^{2+} \quad (2')$$

Correspondingly, Labaki *et al.* [13] mention the absence of Zr^{3+} ions studying coprecipitated copper-zirconia system. In this case, the presence of Cu^{2+} in the bulk must prevent the reduction of Zr^{4+} into Zr^{3+}. Finally, let us note that nitrates can not interact with Zr^{4+} because these ions were eliminated by washing before the heating (see the experimental part).

The direct impregnation of $Fe(NO_3)_3$ on $ZrO(OH)_2$ seems not provide the same interaction as that observed with impregnation of $Fe(NO_3)_3$ on ZrO_2 since the quantity of Zr^{3+} created during the heating seems to be similar to that observed for pure $ZrO(OH)_2$. This result is consistent with XPS result which suggests that, for $Fe/ZrO(OH)_2$ sample, Fe_2O_3 forms preferentially blocks of different height and consequently the initial contact between $Fe(NO_3)_3$ and $ZrO(OH)_2$ is probably weak. But some iron species should interact with ZrO_2 matrix since a delay of zirconia crystallization was observed for this preparation (crystallization temperature higher of 5 and 27°C for respectively $x = 0.01$ and $x = 0.11$). So a small layer of solid solution containing zirconia and Fe^{3+} in low concentration is probably formed during the calcination of $Fe/ZrO(OH)_2$ and leads to the delay of solid crystallization.

Finally it must be pointed out that at 1000°C (excepted for Fe-Zr sample), the same relative amount of Zr^{3+} was obtained. So at this temperature, the main mechanism of defect creation is connected to the zirconia structure (pure monoclinic), iron species deposited at the surface having no influence, certainly because of the drop of the specific area.

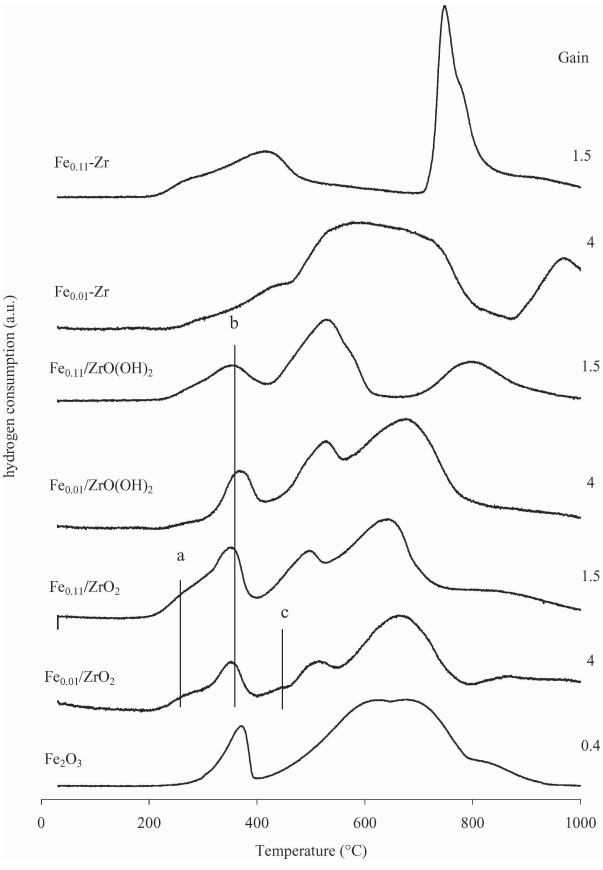

Figure 8 TPR profiles of Fe_2O_3, Fe_x/ZrO_2, $Fe_x/ZrO(OH)_2$ and Fe_x-Zr calcined at 600°C.

As previously mentioned EPR technique allows to evidence at least 2 types of iron species : isolated Fe^{3+} and Fe^{3+} in interaction. But EPR measurements can not detected the entire iron species because some of them may be in antiferromagnetic interaction or in diamagnetic state.

H_2-TPR could confirm the presence of different types of iron species (isolated Fe^{3+}, small or large particles) obtained from the three preparations. In order to make easier the attribution H_2-TPR experiment of standard substance Fe_2O_3 (type α evidenced by XRD analysis) was first performed (Fig. 8). It is well known that the reduction of bulk Fe_2O_3 by hydrogen proceeds through the following steps:

$$3Fe_2O_3 + H_2 \rightarrow 2Fe_3O_4 + H_2O \qquad (5)$$

$$2Fe_3O_4 + 2H_2 \rightarrow 6FeO + 2H_2O \qquad (6)$$

$$6FeO + 6H_2 \rightarrow 6Fe + 6H_2O \qquad (7)$$

In these three processes, the ratio of hydrogen consumptions is 1:2:6. For bulk α Fe_2O_3, TPR profiles exhibit a maximum in H_2 consumption at about 360°C. This peak could be easily attributed to the partial reduction of Fe_2O_3 into Fe_3O_4 (step (5)) since the resultant H_2 consumption corresponds to 11% of total H_2 consumption. At higher temperatures broader peaks are attributable to the reduction of Fe_3O_4 into metallic Fe (steps (6) and (7)). TPR profiles of samples Fe_x/ZrO_2, $Fe_x/ZrO(OH)_2$ and Fe_x-Zr calcined at 600°C are also exhibited in Fig. 8. With respect to that observed on

bulk Fe_2O_3, the reduction of Fe^{3+} species in the presence of zirconia shown significant variations. TPR profiles change with the iron content in the solid but also with the method of preparation. With regard to H_2-TPR obtained with the standard Fe_2O_3, the reduction peak maximum at 340°C (signal "b") observed in all the impregnated samples (Fe_x/ZrO_2 and $Fe_x/ZrO(OH)_2$) can easily attributed to the reduction of bulk Fe_2O_3, phase identified by XRD and Raman spectroscopy. Moreover for the same samples a shoulder at around 275°C is present indicating the reduction of some iron species at a lower temperature. Using H_2-TPR and Mossbauer technique, Chen *et al.* [31] proposed that three different iron species exist on the surface of Fe_2O_3/ZrO_2 catalysts : small Fe_2O_3 particles, bulk phase Fe_2O_3 and surface iron oxide species. Reduction of the small Fe_2O_3 particles is easier than that of the bulk Fe_2O_3 phase, surface iron species being much more difficult to reduce because of their strong interaction with the support. So the shoulder at 275°C (signal "a") can be attributed to the reduction of small Fe_2O_3 particles. This contribution is more significant for Fe_x/ZrO_2 than for $Fe_x/ZrO(OH)_2$. This result can be connected to XRD, Raman spectroscopy and XPS results which evidenced a higher dispersion of iron species in Fe_x/ZrO_2 than in $Fe_x/ZrO(OH)_2$. The presence of surface iron species in strong interaction with zirconia can be suggested for $Fe_{0.01}/ZrO_2$ since an additional maximum of reduction at 450°C (signal "c) is observed in comparison with bulk Fe_2O_3. The H_2-TPR profiles from the coprecipitated samples are very different from those observed from the impregnated samples. For the both samples and according to XRD and Raman results, the absence of bulk phase Fe_2O_3 is confirmed by the lack of signal "b". A strong interaction of iron species with zirconia matrix is observed for $Fe_{0.01}$-Zr since the total reduction of Fe^{3+} into Fe^0 is not complete at 1000°C. The more difficulty to reduce iron species can be connected to the bulk dispersion of these species in the zirconia matrix. Besides, for $x = 0.11$, the first signal observed between 200 and 500°C can be attributed to the reduction of Fe^{3+} into Fe^{2+} (steps 5 and 6 corresponding to 33% of total H_2 consumption) whereas the second peak can be ascribed to the reduction of Fe^{2+} into Fe^0 (step 7).

4. Conclusion

Zirconia-iron samples have been synthesized from three different methods.

In the case of the coprecipitated samples, a delay of zirconia crystallization temperature was evidenced as a function of iron content. At room temperature, the tetragonal phase of zirconia was stabilized. Even low content of Fe^{3+} ions well dispersed in the zirconia prevented Zr^{3+} defects formation whatever the temperature of calcination. In fact the reduction of Fe^{3+} by the released electrons is probably favored in comparison with the reduction of Zr^{4+}.

The direct impregnation of $Fe(NO_3)_3$ on $ZrO(OH)_2$ provided a less stabilization of zirconia structure in the tetragonal phase which could be first explained by a very poor dispersion of iron species since Fe_2O_3 phase was clearly evidenced at very low content of iron in the sample. As a consequence poor interaction between iron and zirconia was also established.

On the contrary, in the case of Fe_x/ZrO_2 sample, interaction of iron precursor with the surface of zirconia was demonstrated : production of surface Zr^{3+} ions was found at low temperature of calcination and explained by the reaction of NO_3^- with Zr^{4+}.

The reduction of iron species is strongly dependant of the synthesis method. The impregnated samples led to the formation of small Fe_2O_3 particles, bulk phase Fe_2O_3 and surface iron oxide species (Fe_x/ZrO_2) whereas the coprecipitated sample led rather to isolated and Fe^{3+} in interaction well dispersed in the bulk and more difficult to reduce.

Acknowledgment

The authors are grateful for the financial support from the "Region Nord-Pas de Calais", the "Conseil Général du Nord" and INTERREG IIIa France-Wallonie-Flandre program (FEDER).

References

1. J. M. HERMANN, J. DISDIER and P. PICHAT, *J. Chem. Soc. Faraday Trans.* **77** (1981) 2815.
2. J. A. NAVIO, G. COLON, M. MACIAS, P. J. SANCHEZ-SOTO, V. AUGUGLIARO and L. PALMISANO, *J. Mol. Cat. A: Chem.* **109** (1996) 239.
3. T. YAMAGUCHI, *Catal. Today* **20** (1994) 199.
4. G. L. MARKARYAN, L. N. IKRYANNIKOVA, G. P. MURAVIEVA, A. O. TURAKULOVA, B. G. KOSTYUK, E. V. LUNINA, V. V. LUNIN, E. ZHILINSKAYA and A. ABOUKAÏS, *Coll. and Surf. A: Physicochem. Eng. Aspects* **151** (1999) 435.
5. W. CAO, O. K. TAN, J. S. PAN, W. ZHU and C. V. GOPAL REDDY, *Mat. Chem. and Phys.* **75** (2002) 67.
6. G. STEFANIC, B. GRZETA and S. MUSIC, *Mater. Chem. Phys.* **65** (2000) 216.
7. F. R. VAN DEN BERG, M. W. J. CRAJÉ, A. M. VAN DER KRAAN and J. W. GEUS, *Appl. Catal. A: General* **242** (2002) 403.
8. Y. OKAMOTO, T. KUBOTA, Y. OHTO and S. NASU, *J. Catal.* **192** (2000) 412.
9. C. Y. HSU, C. R. HEIMBUCH, C. T. ARMES and B. C. GATES, *J. Chem. Soc. Chem. Commun.* (1992) 1645.
10. Y. OKAMOTO, T. KUBOTA, Y. OHTO and S. NASU, *J. Phys. Chem. B* **104** (2000) 8462.
11. T. K. CHEUNG, J. L. D'ITRI and B. C. GATES, *J. Catal.* **151** (1995) 464.
12. E. A. GARCIA, E. H. RUEDA and A. J. ROUCO, *Appl. Catal. A: General* **210** (2001) 363.
13. M. LABAKI, J. F. LAMONIER, S. SIFFERT, E. A. ZHILINSKAYA and A. ABOUKAÏS, *Coll. and Surf. A: Physicochem. Eng. Aspects* **227** (2003) 63.
14. M. J. PEREZ-ZURITA, M. CIFARELLI, M. L. CUBEIRO, J. ALVAREZ, M. GOLDWASSER, E. PIETRI, L. GARCIA, A. ABOUKAÏS and J. F. LAMONIER, *J. Mol. Catal. A: Chemical* **206** (2003) 339.
15. T. SATO, T. ENDO, M. SHIMADA, T. MITSUDOME and N. OTABE, *J. Mater. Sci.* **26** (1991) 1346.
16. J. MATTA, J. F. LAMONIER, E. ABI AAD, E. A. ZHILINSKAYA and A. ABOUKAÏS, *Phys. Chem. Chem. Phys* **1** (1999) 4975.
17. V. S. ESCRIBANO, E. F. LOPEZ, M. PANIZZA, C. RESINI, J. M. G. AMORES and G. BUSCA, *Solid State Sci.* **5** (2003) 1369.

18. V. G. KERAMIDAS and W. B. WHITE, *J. Am. Ceram. Soc.* **57** (1974) 22.
19. N. PANAGOPOULOS, *Thin Solid Films* **137** (1986) 135.
20. P. E. WEST and P. M. GEORGE, *J. Vac. Sci. Technol.* **A 5** (4) (1987) 1124.
21. D. D. SARMA and C. N. R. RAO, *J. Electron Spectrosc. Relat. Phenom.* **20** (1980) 25.
22. C. R. BRUNDLE, T. J. CHUANG and K. WANDELT, *Surf. Sci.* **68** (1977) 459.
23. C. S. KUIVILA, J. B. BUTT and P. C. STAIR, *Appl. Surf. Sci.* **32** (1988) 99.
24. C. D. WAGNER, D. A. ZATKO and R. H. RAYMOND, *Anal. Chem.* **52** (1980) 1445.
25. V. I. DIMZA, *Phys. Status Solidi A* **140** (1993) 543.
26. E. A. ZHILINSKAYA, G. DELAHAY, M. MAUVERZIN, B. LECOCQ and A. ABOUKAÏS, *Langmuir* **19** (2003) 3596.
27. M. J. TORRALVO, M. A. ALARIO and J. SORIA, *J. Catal.* **86** (1984) 473.
28. J. W. FERGUS, *J. Mat. Sci.* **38** (2003) 4259.
29. N. SERGENT, J. F. LAMONIER and A. ABOUKAÏS, *Chem. Mater.* **12** (2000) 3830.
30. F. R. CHEN, G. COUDURIER, J. F. JOLY and J. C. VEDRINE, *J. Catal.* **143** (1993) 616.
31. K. D. CHEN, Y. N. FAN, Z. HU and Q. J. YAN, *Catal. Lett.* **36** (1996) 139.

Received 21 April
and accepted 20 September 2004